LPC CAEN

LABORATOIRE DE PHYSIQUE CORPUSCULAIRE

ISMRA - Boulevard Maréchal Juin - 14050 CAEN CEDEX - FRANCE

Investigating the Nuclear Caloric Curve with a Sequential Statistical Model

A. Siwek, D. Durand, F. Gulminelli, J. Péter

September 1997 LPCC 97-16

Submitted to Physical Review C

INSTITUT NATIONAL
DE PHYSIQUE NUCLEAIRE ET DE PHYSIQUE DES PARTICULES

CENTRE NATIONAL DE LA RECHERCHE SCIENTIFIQUE

INSTITUT DES SCIENCES
DE LA MATIERE ET DU RAYONNEMENT

Téléphone : 02 31 45 25 00
Télécopie : 02 31 45 25 49

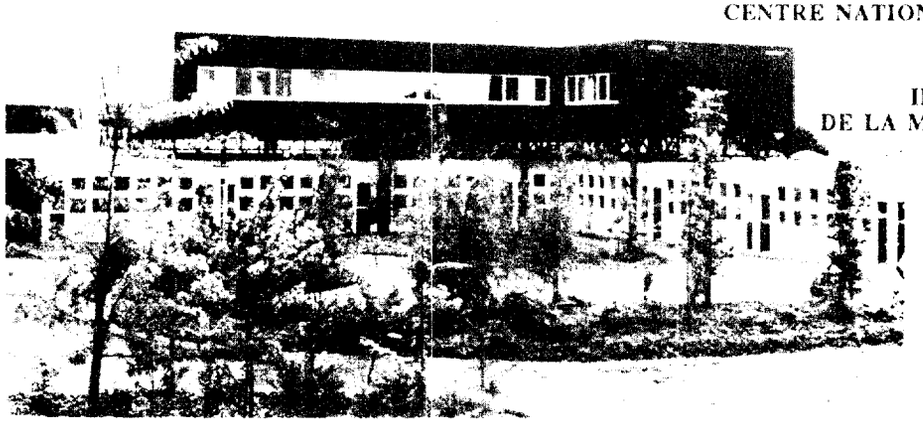

Investigating the Nuclear Caloric Curve with a Sequential Statistical Model

A. Siwek[1,2,*], D. Durand[1], F. Gulminelli[1], J. Péter[1]
[1] *LPC Caen (IN2P3-CNRS/ISMRA et Université), Boulevard du Maréchal Juin, 14050 Caen, France*
[2] *Institute of Nuclear Physics Radzikowskiego 152, 31-342 Cracow, Poland*

The correlation between apparent nuclear temperatures, derived from experimental data, and the initial temperature of excited nucleus was studied within a sequential statistical model. Apparent temperatures were calculated via three methods : 1) inverse slope parameters of kinetic energy spectra of light charged particles, 2) relative population of excited states, and 3) double isotopic yield ratios. Due to the chain of subsequent emissions and side-feeding (decay of particle unstable states) the various apparent temperatures strongly differ from each other and from the initial temperature. In addition, it was found that the model of statistical evaporation is able to reproduce most of INDRA and ALADIN data, even at high excitation energies. This may mean that the apparent temperatures are essentially determined by the statistical nature of the decay of the hot nucleus and its primary fragments.

25.70.Mn,24.10.Pa

I. INTRODUCTION

The thermodynamic properties of hot nuclei have been experimentally studied with increasing temperatures over the years. The relationship between excitation energy E^*, the mass A and the temperature T ("the caloric curve") was found to follow the Fermi gas law, $E^* = a\,T^2$, up to E^*/A =6-7 MeV/nucleon with the constant level density parameter a evolving in the range A/13 to A/8 MeV^{-1} [1]. A caloric curve for nuclear matter over a wider excitation energy range was measured by the ALADIN group [2]. The variation of the temperature with excitation energy exhibits a behavior which has been interpreted as an experimental evidence of a liquid-gas phase transition. Many aspects of the temperature measurements have been discussed recently. The questions of the method reliability [3,4], feeding from particle stable [5,6] and unstable states [4,6–8] an influence of evaporation chain [9] and the physical meaning of the plateau and rise observed [10,11] have been raised. New experimental data have been published [12–15] and made the discussion even more exciting as there are significant differences between these results. Whatever one chooses the same system, the same emitter or the same method, differences are always encountered.

The results of the ALADIN group obtained from the population of excited states of ^{4}He and ^{5}Li [14–17] show temperatures as low as 4-5 Mev in collisions of Au + Au at 600 MeV/nucleon whereas the double isotopic yields ratio ^{6}Li/^{7}Li-^{3}He/^{4}He indicated temperatures up to 9 MeV. A similar situation is faced by the INDRA collaboration for the systems Ar+Ni at 52-95 MeV/nucleon [12] and Xe+Sn at 50 MeV/nucleon [18] : different double isotopic yield ratios give different temperature values, slope parameters indicate larger values, excited state populations produce lower values [19]. The same double isotopic ratio (^{6}Li/^{7}Li-^{3}He/^{4}He) used by both groups (INDRA and ALADIN) to determine the temperature gives similar values, however the caloric curves are different: a plateau followed by a steep increase of T above E^*/A= 10 MeV/nucleon was found in [2] whereas a steadily increasing slope of T versus E^*/A was obtained in [12]. And finally the EOS data [13,20] obtained for Au projectile do not agree with the ALADIN data at the highest excitation energies measured (10-15 MeV/nucleon).

This puzzling picture rises the question of the relationship between these different apparent temperatures and the initial one. Apart from dynamical effects, two mechanisms influence the apparent temperature:

1. Emission chain - the excited nucleus lowers its temperature after each act of emission. This applies also to fragments emitted into excited states in the continuum. The higher is the excitation energy the longer is the emission chain and in consequence the bigger is the discrepancy between initial and apparent emission temperatures.

2. Decay of particle unstable levels (side-feeding) - This removes the parent fragment from measurement and increases the number of daughter particles, influencing also their kinetic energy spectra and the population of their

*Present address: University of Lund, KOSUFY, Box 118, 22100 Lund, Sweden.

ground and excited states. The probability of reaching particle unstable levels increases with excitation energy. In this paper we attempt to establish quantitatively these respective effects within the standard evaporation model. We compare our results with INDRA [12,19] and ALADIN [2,14] experimental data.

The paper is organized as follows. In Sec.II we shortly describe the available methods of temperature determination from charged particles measurements. Sec III presents the model and the way theoretical results were analysed. The temperatures calculated at various stages of the de-excitation process are presented in Sec.IV. In Sec.V we discuss the influence of the level density parameter and of the maximum width of included excited states. In Sec. VI, the results are compared to experimental data. Conclusions are presented in Sec.VII.

II. METHODS TO MEASURE NUCLEAR TEMPERATURE

For convenience, the methods of temperature determination from measurements of charged products will be called respectively kinetic, isotope (or chemical) and population temperatures in this paper.

A. Slope parameters, kinetic temperature T_s.

This most widely used method to determine a temperature of nuclei is based on measurements of kinetic energy spectra of emitted particles. A nucleus in thermal equilibrium evaporates particles with an energy distribution defined by the Maxwell-Boltzmann formula:

$$N(E_k) = C * (E_k - B_c) \exp - \frac{(E_k - B_c)}{T_s}, \tag{1}$$

where E_k is the kinetic energy of the emitted particle, Bc is the Coulomb barrier, and T_s the temperature of the source after emission.

The main problem in applying this formula to the experimental data is to define the emitting source properly. One can do it in three different ways :

- by coincidence measurements of emitted particles with evaporation residues [21] or fission fragments [22] - This method is applicable at low incident energies where fusion is the dominant process and only one heavy residue exists in each event.
- by "three sources fit" of inclusive spectra at several detection angles. - Events issued from a broad range of impact parameters and excitation energies are analyzed together; the averaging of different source velocities produces a distortion of the spectra which leads to erroneously high slope parameters [23,24].
- by reconstruction of the source(s) in each event. - This is the only reliable method applicable at incident energies above 15-20 MeV/nucleon where two main hot sources (quasi-projectile and quasi-target, or spectators) are accompanied by mid-rapidity emission (direct emission, neck emission or participants). The full impact parameter range corresponds to the formation of hot nuclei on a broad excitation energy range. This makes it possible to measure a full caloric curve with a single system at one incident energy [2,12,18] but the method requires an almost complete detection of particles and fragments emitted by the selected source (fusion, or quasi-projectile [25,26] or quasi-target)

B. Double isotopic ratio, T_r^0

This method was proposed in 1989 [27] and recently attracted much attention when it was used by the ALADIN group [2] to study the dependence of the temperature on the excitation energy. The method starts from the assumption of thermal and chemical equilibrium of the emitter. Then the ratio between the yields of two isotopes (isotones) differing by one proton (neutron) depends only on the temperature and the free proton (neutron) density. In the ratio of two such ratios the proton (neutron) density cancels out and the double ratio is only depending on the temperature through the simple formula [27],

$$T_r^0 = B / \ln \left(s \cdot \frac{Y_1/Y_2}{Y_3/Y_4} \right), \tag{2}$$

where Y_1, Y_2, Y_3, Y_4 - are the yields of the four isotopes,
s depends on the spins of the populated states of each species,
and B is the difference of binding energy differences $(B2 - B1) - (B4 - B3)$.

When, as assumed in the original paper, there are no low lying excited states, the calculation of s can include only ground state spins. This approximation is valid at low temperatures (a few MeV). At higher temperatures, the population of excited states should be taken into account, which means s depends on T_r and on the number of states included. Since experiments cannot measure the population of all excited states and since one wants to keep the simplicity of the formula, all detected nuclei are taken as if they had been emitted in their ground state. This approximation has non-negligible effects above 5 MeV and is indicated by the index 0: T_r^0.

The larger the value of B, the better the sensitivity of T_r^0. Therefore we will study only three cases where the pair of isotopes at the denominator is ^{3}He-^{4}He.

C. Relative population of excited states, T_{pop}.

The principle of this method is the fact that a nucleus in thermal equilibrium emits clusters into states 1 and 2 with a relative probability proportional to the Boltzman factor:

$$F_B = \exp \frac{-\Delta E^*}{T_{pop}}, \tag{3}$$

where $\Delta E^* = E_1^* - E_2^*$ is the energy difference between states 1 and 2 (state 2 is often the ground state), and T_{pop} is the temperature of the source.

The ratio between the number of clusters emitted in two different states is :

$$\frac{N_1}{N_2} = \frac{2J_1 + 1}{2J_2 + 1} * F_B, \tag{4}$$

where N_1, N_2 are the numbers of fragments emitted in states 1 and 2, respectively, and J_1, J_2 are their spins. From these equations, the population temperature is given by:

$$T_{pop} = \frac{\Delta E^*}{ln \frac{2J_2+1}{2J_1+1} \frac{N_1}{N_2}} \tag{5}$$

This method is sensitive enough only when the value of ΔE^* is much larger than the temperature. It was used especially by a MSU group [24,28–30]. Both particle stable and unstable states were used. The values obtained were called emission temperatures, but we will see they are sensitive to decay chain and side-feeding and may have largely lost the memory of the temperature at the moment they were emitted. The values obtained in this way are much lower than those extracted from slopes of kinetic energy spectra. Values about 4-5 MeV were extracted and seem to be insensitive to the type of reaction and slightly increasing with increasing bombarding energy [31].

III. THE MODEL

The standard evaporation theory was applied to model the excited nucleus decay [32]. The basic hypothesis of this model is that the successive emissions are independent of each other (except for the decrease in excitation energy, temperature and angular momentum), i.e. the source re-establishes a full thermal equilibrium after each emission. One may argue this is no longer valid when the temperature is so high that successive emissions occurs within very short times (a few 10^{-22} s). Nevertheless we kept this hypothesis in order to fully investigate what can be obtained within such a model. The role of angular momentum was not studied here.

In the calculations fragments with Z<6 and A<10 are emitted in discrete states. Heavier fragments decay until the excitation energy is exhausted or until they decay into fragments with Z<6 and A<10. All discrete states decay at the end of calculation. The total excitation energy is chosen randomly and the initial temperature, T_{ini}, is calculated from the Fermi gas formula with $a = A/10$: $T_{ini} = \sqrt{10 * E^*/A}$, as well as the temperature T at each step of the de-excitation chain. This is merely an example and another value of a or a different variation of T_{ini} and T with E^*/A can be introduced.

All discrete states for which excitation energy, spin and width are known were included in the code [33]. The maximum width of the states included in the calculations is a free parameter.

A. Technical details

T_r^0 and T_{pop} require only to count the number of particles of different types or the relative population of different states, respectively. T_s needs the velocities and is then sensitive to recoil effects. All particle velocities are relative to the initial location in momentum space of the excited nucleus. For the first emission, the velocity in the initial location frame is the same as in the emitter frame. For subsequent emissions, the emitter has shifted from its initial location and the particle velocity in the initial location frame is larger, on the average, than in the emitter frame. Successive recoil effects increase kinetic energies especially for heavy particles which have lower velocities. Indeed, in thermal emission, the kinetic energy spectra in the emitter frame are the same for all particles (except below the Coulomb barrier), so light particles get larger velocities than heavy ones. At the same time, of course, the temperature decreases and the kinetic energy in emitter frame decreases.

B. Successive steps

To understand the influence of emission chain and side-feeding on apparent temperature we stopped the calculations at different stages. The details of this procedure are described below.

- Emission Chain - The temperature of the emitter decreases continuously at each successive emission. In order to study the nucleus at a well defined temperature we stopped the calculations after the first emission step. We call this First Chance Emission (FCE) in contrast to Evaporation Chain (EC) where the full chain of evaporations is included.
- Side feeding - Due to decay of particle unstable states the final yields, kinetic energy distributions and excited state populations relative to the ground state population differ from the initial distributions of particles emitted by the source. To get rid of this effect we disabled the decay of discrete levels for both FCE and EC calculations. They will be referred to as "before decay". Consequently the calculations with the decay of discrete levels enabled will be called "after decay".
- Ground state (g.s.) selection - To use isotope thermometers in the right way with formula (2), only fragments emitted in the ground state should be taken into account (see section 2.3). For this reason the calculations "before decay" were divided into two separate classes: "g.s. only" and "all states" (where all excited states are included).

IV. RESULTS

In this section we show the results of calculations made for nuclei similar to the quasi-projectiles (QP) produced in the reaction Ar + Ni at 95 MeV/nucleon. Following the experimental data, the charge of the QP is between Z=12 and 20 with a gaussian distribution centered at Z=16. The variance is excitation energy dependent and changes from σ=0. for E*=0 to σ=1.56 for E*=20MeV/nucleon. The average mass was chosen to be equal to twice the charge in order to keep the charge-to-mass ratio equal to that of the projectile. We will analyse changes in the apparent temperature values through the steps described above.

A. FCE before particle's decay - test of the model

In the FCE calculations only one particle (fragment) is emitted from the source which has well defined temperature and excitation energy. The fragment does not decay even if it is emitted in an excited state. The apparent temperatures calculated from both energy spectra and relative yields are expected to be very close to the initial one.

"g.s. only". As mentioned in the previous section, to calculate isotope temperatures correctly we have to take into account only particles emitted in their g.s. This stage of calculation is a test of the code. The results are shown in Fig.1.

The temperatures calculated from the slopes of energy spectra are slightly lower than the initial value. This reflects the fact that the temperature in formula (1) is that of the nucleus remaining after fragment emission, slightly lower than the initial one. The difference is larger for temperatures obtained from double isotopic ratio.

"all states". All fragments (g.s. + excited) are used. Of course, the kinetic temperatures remain unchanged (Fig.2a). The isotope temperatures decrease at high T_{ini} (Fig.2b). This means that already at this stage the approximations on s in Albergo's formula have a significant effect. Excited states populations also give temperature values which are close to the initial ones (Fig.2c).

B. FCE after particle decay (side-feeding).

If we go one step further and allow excited particles to decay, we can study the influence of secondary decays on the measured temperatures. The results are shown in Fig.3. Side-feeding has little influence on the energy spectra, therefore the slopes remain unchanged (Fig.3a). The decrease in isotope temperature (Fig.3b) is caused mainly by the increase in the number of α-particles since : i) there is very weak increase in the yield of d,t and ^{3}He, and ii) the changes in the number of ^{6}Li and ^{7}Li approximately compensate each other. The population temperatures depend on the isotope used (Fig.3c). The apparent temperature obtained from ^{5}Li keeps a good memory of the initial one while that from ^{8}Be is very much affected by side-feeding and reaches only half the initial value when $T_{ini} > 10$ MeV. One should notice that such a dramatic effect is obtained in spite of the choice of very large values of ΔE^*.

C. Evaporation chain before particle decay

The calculations with the full evaporation chain go through the same steps as for first chance. The evaporation chain ends when the excitation energy of fragments with A>9 and Z>5 is exhausted.

"g.s. only". The result is shown in Fig.4. By comparing it to Fig.1 and Fig.3 , one sees that the influence of the evaporation chain is stronger than the side-feeding effect in the FCE scenario. Kinetic temperatures are generally lower than the initial ones (Fig.4a), as expected since the temperature decreases along the chain.

However, T_s tends to reach the initial value at the highest excitation energies. This is due to successive recoil effects which, on the average, increase the velocities of late particles in the initial location frame. For isotope temperatures, formula (2) is fully correct since only fragments emitted in the ground state are used. Two of the studied isotopic ratios increase almost linearly and their apparent temperatures stay well below T_{ini} (Fig.4b). The other one, obtained from ^{6}Li/^{7}Li-^{3}He/^{4}He, behaves quite differently: above $E^*/A \approx 7$ MeV/nucleon it increases fast and becomes larger than the initial temperature around 11 MeV/nucleon. This is caused by much faster increase of the yields of ^{3}He and ^{7}Li as compared with ^{4}He and ^{6}Li.

"all states". The inclusion all excited states in the temperature calculation does not change much the picture. A further weak decrease in the isotope temperatures is observed (Fig.5b). The curve for ^{6}Li/^{7}Li-^{3}He/^{4}He becomes identical to the two other curves up to $E^*/A \approx 9$ MeV/nucleon. At this stage population temperatures can also be calculated: Fig.5c. The effect of the de-excitation chain is seen by comparing it to Fig.2c: a strong decrease is observed at excitation energies above 5 MeV/nucleon.

D. Evaporation chain after particle decay

This is the final step in the de-excitation process. At this point the side-feeding effect is added to the evaporation chain effect. The results are shown in Fig.6. The kinetic temperatures do not change, except for ^{6}Li which exhibits a strong increase at very high excitation energies (Fig.6a). This is due to the additional recoil when a fragment emits a particle. One notices a further strong decrease in the isotope temperature (Fig.6b), caused mainly by the increase in the number of alpha particles. Still the shape of the curve obtained from ^{6}Li/^{7}Li-^{3}He/^{4}He ratio remains different from the other two ratios. The behavior of the population temperature depends on the cluster: Fig.6c. One sees a strong decrease in the case of ^{4}He over a wide excitation energy range (again due to the large number of α-particles emitted in the ground state when heavier clusters decay) and a small effect in the case of ^{5}Li. The most dramatic effect is a flattening of the curve for ^{8}Be, which becomes almost insensitive to T_{ini} above 5 MeV.

V. DISCUSSION

The slope parameters from kinetic energy spectra of light particles keep a good memory of the initial temperature. Note however that in an actual experiment they may be perturbed by the contribution of another source; the possible contribution of collective expansion should also be considered.

Both emission time sequence and feeding from discrete state decays have large effects on caloric curves measured with isotope thermometers. Secondary decays (side-feeding) reduce the apparent temperature values while the emission chain changes the shape of the caloric curves. For the Li-He thermometer these effects produce a shape that could easily mimic a liquid-gas phase transition (Fig.6c; see also Fig.8 and 9).

Most of the population temperatures are very sensitive to side-feeding effects. They stay constant over a wide range of excitation energy and have values as low as 3-5 MeV. The only exception is ^{5}Li.

One should keep in mind that isotope and population temperatures are sensitive to the characteristics of the levels used. We have taken into account existing information, which may be incomplete or inaccurate. Any missing (or extra) level, error on spin assignment or on the branching ratio into particle decay of fragments with mass greater than 4 may have a very significant effect.

A. Sensitivity of the final results on the input parameter variation

There are no free parameters in the code adjustable to experimental data. However two physical variables, used as inputs, can influence the results:

- the number of discrete excited states included in the calculation, which is governed by a cut-off width, Γ : only states with a width smaller than Γ are taken into account.
- the level density parameter, which defines the very important relation between temperature and excitation energy.

The value of both parameters is in principle excitation energy dependent. We did not try to introduce such kind of dependence; instead we show calculations for three different values selected within physically reasonable ranges.

1. Width of excited states

Having the width of each discrete state included in the code we can study the influence of in(ex)cluding some of the states. In Fig.7 we present results obtained by including states with $\Gamma < 0.5$, 2.0 and 4.0 MeV (which correspond to life times > 400, 100 and 50 fm/c, respectively). There is almost no difference between $\Gamma < 2.0$ MeV and $\Gamma < 4.0$ MeV; only $\Gamma \ll 0.5$ MeV produces a difference.

The effect on slope parameters is weak. For isotope temperatures, the restriction to states with $\Gamma < 0.5$ MeV gives higher T_γ^0 values than the two other cases. This is caused by a lower number of emitted alpha particles. This effect is also clearly visible in the population temperature from ^{4}He. The other population temperatures are not affected by the limitation on Γ. Note no temperature is obtained for ^{5}Li when $\Gamma < 0.5$ MeV since the ground state width is 1.5 MeV.

2. Level density parameter

There are theoretical calculations [34] and also some experimental evidences [1] on the level density parameter's dependence on excitation energy. To see how its value affects apparent temperatures we made calculations for $a = A/8$, $A/10$ and $A/14$ MeV^{-1}. The results are presented in Fig.8.

Above $T_{ini} \sim 9$ MeV, T_s increases with increasing a. This effect is small for deuterons, but clear for He and Li clusters. It is due to recoil effects: large a values correspond to high values of E^*/A, hence to more emitted particles and more cumulative recoil effects. As noted before, light particles like deuterons have larger velocities in the emitter frame than heavy particles like He or Li and are then much less affected. For He and Li, the broadening of the kinetic energy distribution in the initial location frame relative to the emitter frame can be so large that the slope parameter value can exceed the initial temperature.

^{6}Li/^{7}Li-^{3}He/^{4}He isotopic temperature are affected by variation of the level density parameter. The difference becomes significant above 10 MeV of initial temperature.

Population temperatures are insensitive to the level density parameter.

VI. COMPARISONS TO EXPERIMENTAL DATA.

In the above calculations, the angular momentum, expansion energy and deformation are set to zero for all excitation energies. When using such calculations for comparison with experimental data, one should keep in mind that the nucleus actually formed in a collision may have non-zero values of such quantities. It is also possible that more than

one initial excited nucleus is formed in the reaction. When one of them is selected, the question arises of a possible contribution from other source(s). This is an experimental problem which will not be discussed here and the published data will be used.

This simulation applies to nuclei whose initial charge, mass, excitation energy and location in momentum space are well defined. However in experiments, the velocity of the initial excited nucleus is not known and is reconstructed from its detected charged products event-by-event [25]. Since neutrons usually are not detected, or only a few of them are detected, the center-of-gravity of the detected products does not coincide with the initial location of the excited nucleus. Therefore, in order to get more realistic information on kinetic energy spectra, the same method was used here: the initial position of the excited nucleus was not used, it was reconstructed from the momenta of charged products. This produces an additional broadening of the velocity distributions, and hence an increase of T_s values. But this increase is much smaller than the increase due to successive recoil effects.

A. INDRA data

The calculations above were performed for a system directly comparable to the quasi-projectiles formed in collisions of ^{36}Ar on ^{58}Ni from 52 to 95 MeV/nucleon, having excitation energies up to 24 MeV/nucleon [12,19].

Let us determine the values of the free parameters which give the best agreement with the data : maximum width of excited states and level density parameter.

The role of Γ is shown in Fig.9, for $a = A/10$ MeV^{-1}. To reproduce temperatures from p/d-^{3}He/^{4}He one has to include very broad (short living) states, while d/t-^{3}He/^{4}He requires to exclude states with $\Gamma > 0.5$ MeV. Temperatures from ^{6}Li/^{7}Li-^{3}He/^{4}He suggest a change in the time scale: broader states should be included as excitation energy increases.

The general behavior of the data is well reproduced by the calculations. A quantitative agreement cannot be obtained with an unique value of Γ, but one has to keep in mind that the widths, spins and branching ratios of many excited states are poorly known. A reasonable overall fit is obtained with $\Gamma < 2.0$ MeV; this value was used for studying the sensitivity to a.

In Fig.10, one can see that the value chosen for the level density parameter a does not drastically changes the agreement with the data.

The slope parameters of deuterons are well reproduced with $a = A/8$ or $A/10$ MeV^{-1}. For ^{4}He and ^{6}Li the slope of T_s versus E^*/A is better reproduced by $a = A/14$ MeV^{-1}, but T_s values are underestimated. This discrepancy could be attributed to collective effects (expansion) which may be present in the data and increase the kinetic energies and T_s for fragments with mass 4 and 6 while they would affect weakly mass 2. Alternatively, if expansion is not present, a variation of a from $A/14$ at low excitation energies to $A/8$ or $A/10$ MeV^{-1} at high excitation energies would better reproduce the data, in agreement with the variation of a with E^*/A observed below 7 MeV/nucleon [1].

Isotope temperatures from p/d-^{3}He/^{4}He and ^{6}Li/^{7}Li-^{3}He/^{4}He are reasonably well reproduced by all 3 values on the whole range of excitation energies, while d/t-^{3}He/^{4}He is underestimated above 10 MeV/nucleon.

The calculated population temperatures of ^{5}Li are overestimated above 10 MeV/nucleon.

In the simulation shown in Fig.1-6, $\Gamma < 2.0$ MeV and the level density parameter $a = A/10$ MeV^{-1} were used.

B. ALADIN data

To check the scenario of sequential statistical decay on heavier nuclei, we made calculations for ALADIN data [2,14] as well. Indeed the system was Au on Au at higher bombarding energies (600 MeV/nucleon), and heavier excited QP's were formed. The other difference is the QP mass decreases strongly as the excitation energy increases while for Ar projectile QP's with an approximately constant mass were selected.

In the data analysis, temperatures were extracted using one double yield ratio and excited states populations of two isotopes. Like for INDRA data, apparently contradictory values were obtained. The caloric curve from ^{6}Li/^{7}Li-^{3}He/^{4}He [2] reaches $T \approx 10$ MeV while the population temperatures of ^{4}He and ^{5}Li stay constant around 4 and 5 MeV for $10 < E^* < 15 MeV/nucleon$. [14,35].

To adapt the code's inputs to this case, we included the dependence of the source mass on excitation energy (A from 190 to 55 when E^*/A increases from 2 to 15 MeV/nucleon) [2] and an A/Z ratio 2.5 for all E* was assumed. The isotope temperatures obtained for $\Gamma < 2.$ MeV and $a = A/10$ MeV^{-1} are presented in Fig.11. The theoretical calculations were multiplied by 1.2, since this factor was applied to experimental data [2]. Both the shape and the absolute value are reproduced, but for the highest excitation energy. The temperature from ^{5}Li excited states is shown in Fig.12. The model predicts apparent temperatures 2-3 MeV too high, like for INDRA data. The population

temperatures calculated for ^{4}He ^{6}Li and ^{8}Be are shown on the same figure as well. They are all lower than for ^{5}Li and behaves similar to those calculated for Ar quasi projectile decay.

VII. SUMMARY AND CONCLUSIONS

The simple model of sequential statistical decay (evaporation) which includes emission of excited fragments in discrete states was used to study the effects of emission time sequence and feeding from discrete state decays on various apparent temperatures: kinetic temperatures (slope parameters), isotope or chemical temperatures and population temperatures.

Slope parameters from kinetic energy spectra of light particles keep a good memory of the initial temperature (but in actual experiments they may be perturbed by the mixture of several sources and by collective expansion).

It was found that both the de-excitation chain and side-feeding have large effects on caloric curves measured with isotope thermometers. Secondary decays (side-feeding) reduces apparent temperature values while emission chain changes the shape of the caloric curve for the Li-He thermometer in such a way that it could easily mimic a liquid-gas phase transition. A similar effect was reported by R.Wada [9] for much heavier system (A $\approx$ 230-250) and limited range of excitation energy (up to $\approx$ 5.3 MeV/nucleon).

A specific problem concerns the population temperatures of ^{5}Li. At E^{*}/A above 10 MeV/nucleon, the calculation overestimates them relative to INDRA data as well as to ALADIN data. The fast multifragmentation calculation of ref. [8] also overestimates INDRA data. Actually, experimental temperatures extracted from particle unstable states remain almost constant as a function of excitation energy and do not overcome $\approx$ 5 MeV [14–17]. A possible explanation could be the source is expanding and heavy clusters are formed relatively late during this expansion, at lower temperatures. A support to this view in the INDRA experiment can be found in the kinetic temperatures of He and Li: the measured values are greater than the calculated values (Fig. 9, 10).

Surprisingly, the simple model of sequential statistical emission was found to be able to reproduce the behavior of most apparent temperatures observed in INDRA and ALADIN experiments, even at high excitation energies. This result suggests that the real mechanism of hot nucleus disassembly is weakly related to the apparent temperatures. All of them are essentially determined by subsequent emissions. A confirmation of this point can be found in ref. [8] where the same INDRA experimental data are well reproduced by a quite different model (fast multifragmentation) with the same treatment of side-feeding.

Our results are also in agreement with previous study of side-feeding effect. The saturation of apparent temperature was found [36]for different population temperatures. In case of isotopic temperature the correction factor was applied [37,38] with which the corrected temperatures from different "thermometers" are more consistent. In case of INDRA data this factor do not give an overall agreement between three different isotopic ratios [38] (Li-He temperature remains higher that the other two) and this is exactly what we have found in our calculations.

@@@@@@@@@@@@@@@@@@@@ REFERENCES @@@@@@@@@@@@@@@@@@@@

[1] R. Wada et al., Phys. Rev. C **39** (1989) 497.
[2] J. Pochodzalla et al., Phys. Rev. Lett. **75** (1995) 1040.
[3] X. Campi, H. Krivine, E. Plagnol, Phys. Lett. **B 385** (1996) 1.
[4] A. Kolomiets et al., Phys. Rev. C **54** (1996) R472
[5] M.B. Tsang et al., Phys. Rev. C **53** (1996) R1057.
[6] H. Xi, W.G. Lynch, M.B. Tsang, W.A. Friedman, Phys. Rev. C **54** (1996) R2163
[7] M.J. Huang et al., Phys. Rev. Lett. **78** (1997) 1648
[8] F. Gulminelli, D. Durand, Nucl. Phys. **A615** (1997) 117
[9] R. Wada et al., Phys. Rev. C **55** (1997) 227.
[10] J. Natowitz, K.Hagel, R. Wada, Z. Majka, P.Gonthier, J. Li, N. Mdeiwayeh, B. Xiao, and Y. Zhao, Phys. Rev. C **52** (1995) R2322.
[11] L.G. Moretto, R. Ghetti, L. Phair, K. Tso, and J.G. Wozniak, Phys. Rev. Lett. **76** (1996) 2822.
[12] Ma Y.-G. et al., Phys. Lett. B **390** (1997) 41.
[13] J.A. Hauger et al., Proc. of the 1st Catania Relativistic Ion Studies, Italy, May 1996: CRIS '96, ed. S. Costa et al., World Scientific.
[14] J. Pochodzalla et al., Proc. of the 1st Catania Relativistic Ion Studies, Italy, May 1996: CRIS '96, ed. S. Costa et al., World Scientific.
[15] G. Imme et al., Proc. of the 1st Catania Relativistic Ion Studies, Italy, May 1996: CRIS '96, ed. S. Costa et al., World Scientific.
[16] C. Schwarz et al., Proc. XXXVth Int. Meeting on Nuclear Physics, Bormio, Italy, Feb. 1997, p. 456, ed. I. Iori.
[17] S. Fritz et al., Proc. XXXVth Int. Meeting on Nuclear Physics, Bormio, Italy, Feb. 1997, p. 479, ed. I. Iori.
[18] J. Péter et al., preprint LPC Caen 97-08, Proc. 13th Winter Workshop on Nuclear Dynamics, Marathon, USA, Feb. 1997, World Scientific.
[19] M. Assenard et al., Proc. XXXVth Int. Meeting on Nuclear Physics, Bormio, Italy, Feb. 1997, p. 465, ed. I. Iori.
[20] M.L. Tincknell et al., Advances in Nuclear Dynamics 2, Plenum Press, New York, 1996, p.269
[21] A. Siwek et al., Z. Phys A **350** (1995) 327
[22] H. Wu, G. Jin, Z. Li, G. Dai, Y. Qi, Z. He, Q. Luo, L. Duan, W. Wen, B. Zhang, Nucl. Phys. A **617** (1997) 385
[23] G.D. Westfall et al., Phys. Lett. B **116** (1982) 118.
[24] J. Pochodzalla et al., Phys. Rev. C **35** (1987) 1695
[25] D. Cussol et al., Nucl. Phys. A **561** (1993) 298
[26] J. Péter et al., Nucl. Phys. A **593** (1995) 95
[27] S. Albergo, S. Costa, E. Costanzo and A. Rubbino Nuovo Cimento **A89** (1989) 1.
[28] T.K. Nayak et al., Phys. Rev. C **45** (1992) 132
[29] C. Schwarz et al., Phys. Rev. C **48** (1993) 676
[30] F. Zhu, W.B. Lynch, D.R. Bowman, R.T. de Souza, C.K. Gelbke, Y.D. Kim, L. Phair, M.B. Tsang, C. Williams, and H.M. Xu Phys. Rev. C **52** (1995) 784
[31] G.J. Kunde et al., Phys. Lett. B **272** (1991) 202
[32] D. Durand et al, *in preparation*
[33] Table kindly communicated by J. Konopka and H. Stöcker, completed with widths from F. Ajzenberg-Selove Nucl. Phys. **A320**(1979)1, **449**(1986)1, **475**(1987)1, **506**(1990)1, P. M. Endt Nucl. Phys. **A521**(1990)1, D. R. Tilley et al. Nucl. Phys. **A564**(1993)1
[34] P. Bonche et al., Nucl. Phys. A **427** (1984)278
[35] V. Serfling, Ph D thesis, Frankfurt, 1997
[36] Z. Chen and C.K. Gelbke, Phys. Rev. C **38** (1988) 2630
[37] M.B. Tsang, W.G. Lynch, and H. Xi, Phys. Rev. Lett. **78** (1997) 3836
[38] H. Xi et al., Report MSUCL-1055 January 1997

@@@@@@@@@@@@@@@@@@@ FIGURE CAPTIONS @@@@@@@@@@@@@@@@@@@

FIG. 1. Apparent temperatures as a function of the initial temperature calculated with a sequential statistical code for the first chance emission before secondary decay. Only particles emitted in the ground states were included. a) Temperatures T_s extracted from the slope parameters of kinetic energy spectra of three emitted particles. b) Temperatures T_r^0 extracted from double yield ratios of three pairs of isotopes differing by 1 neutron. Symbols are explained on the Figure.

FIG. 2. Same as Fig.1 (first chance emission before secondary decay), but particles emitted at all levels were included. a) T_s. b) T_r^0. c) Temperatures extracted from excited state populations (T_{pop}) of three products. Symbols are explained in the Figure.

FIG. 3. Same as Fig.2 (first chance emission with all levels), but temperatures calculated after secondary decay.

FIG. 4. Same as Fig.1, but for the full emission chain before secondary decay. Only particles emitted in the g.s. were included. a) T_s. b) T_r^0.

FIG. 5. Same as Fig.4 (full emission chain before secondary decay) but particles emitted at all levels were included. a) T_s. b) T_r^0. c) T_{pop}.

FIG. 6. Same as Fig.4 Full emission chain after secondary decay, i.e. complete calculation.

FIG. 7. Dependence of the calculated apparent temperatures on the maximum width of discrete states Γ included in the calculations. Open circles: $\Gamma < 0.5$ MeV. Dots: $\Gamma < 2$ MeV. Stars: $\Gamma < 4$ MeV. Left column: T_s. Central column: T_r^0. Right column: T_{pop}.

FIG. 8. Dependence of the calculated apparent temperature on the level density parameter a. Open circles: $a = A/8$ MeV^{-1}. Dots: $a = A/10$. Stars: $a = A/14$. Left column: T_s. Central column: T_r^0. Right column: T_{pop}.

FIG. 9. Results of theoretical calculations for different restrictions on the maximum width Γ of discrete states (lines), compared with INDRA data (open circles). Dashed lines: $\Gamma < 0.5$ MeV. Solid lines: $\Gamma < 2$ MeV. Dotted lines: $\Gamma < 4$ MeV. The vertical axis is the apparent temperature (as in Fig.1-8), but the abscissa is the initial excitation energy per nucleon. Left column: T_s. Central column: T_r^0. Right column: T_{pop}.

FIG. 10. Results of theoretical calculations for different values of level density parameter a (lines), compared with INDRA data (open circles). Dashed lines: $a = A/8$ MeV^{-1}. Solid lines: $a = A/10$. Dotted lines: $a = A/14$. The vertical axis is the apparent temperature (as in Fig.1-9), the abscissa is the initial excitation energy per nucleon (as in Fig.9). Left column: T_s. Central column: T_r^0. Right column: T_{pop}.

FIG. 11. Apparent temperature T_r^0 calculated with the code from the double isotopic yields ratio ^{6}Li/^{7}Li-^{3}He/^{4}He (the shaded area represents statistical errors) compared with ALADIN data.

FIG. 12. Apparent population temperatures T_{pop} calculated with the code for different isotopes (the shaded area represents statistical errors) compared with ALADIN data for ^{5}Li.

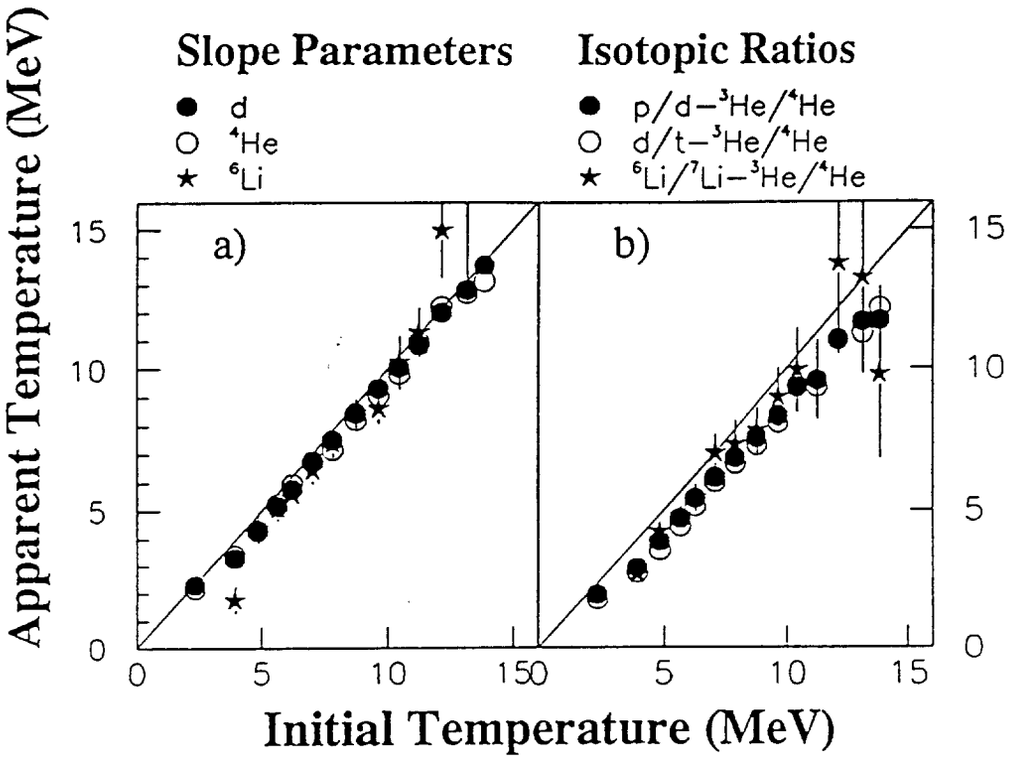
Slope Parameters
d
4He
6Li
Isotopic Ratios
p/d−3He/4He
d/t−3He/4He
6Li/7Li−3He/4He
a)
b)
Apparent Temperature (MeV)
Initial Temperature (MeV)
0
5
10
15

Fig. 1

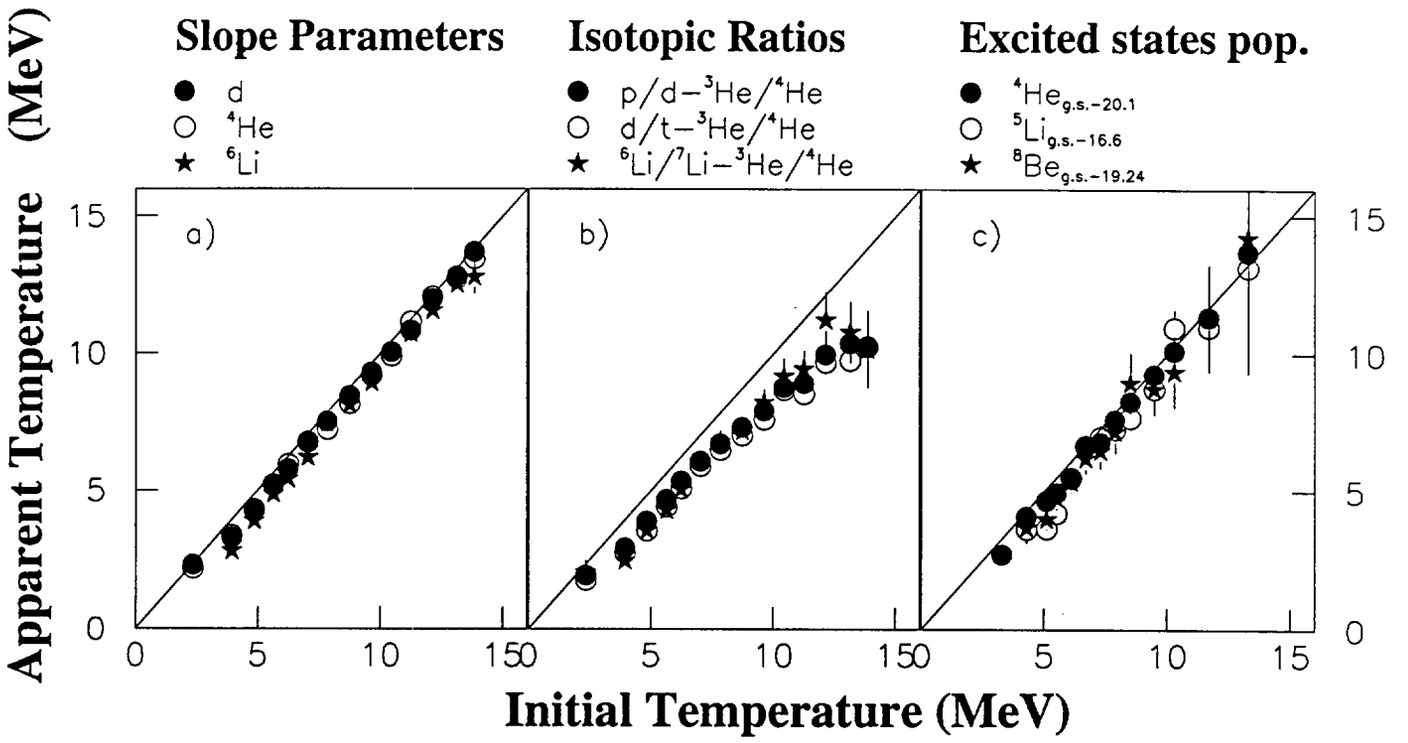
Slope Parameters
d
4He
6Li
Isotopic Ratios
p/d−3He/4He
d/t−3He/4He
6Li/7Li−3He/4He
Excited states pop.
4He g.s.−20.1
5Li g.s.−16.6
8Be g.s.−19.24
a)
b)
c)
Apparent Temperature (MeV)
Initial Temperature (MeV)
0
5
10
15

Fig. 2

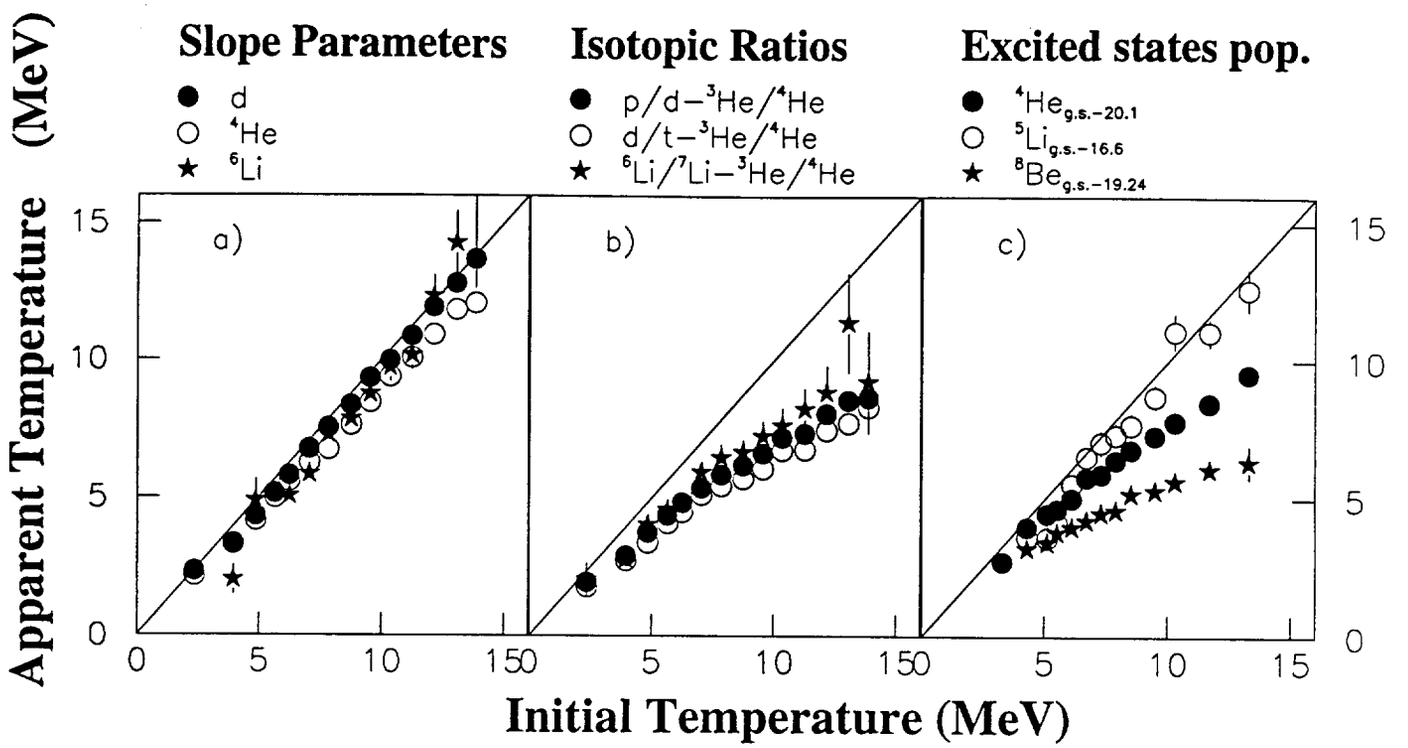
Slope Parameters
d
4He
6Li
Isotopic Ratios
p/d−3He/4He
d/t−3He/4He
6Li/7Li−3He/4He
Excited states pop.
4He g.s.−20.1
5Li g.s.−16.6
8Be g.s.−19.24
a)
b)
c)
Apparent Temperature (MeV)
Initial Temperature (MeV)
0
5
10
15

Fig. 3

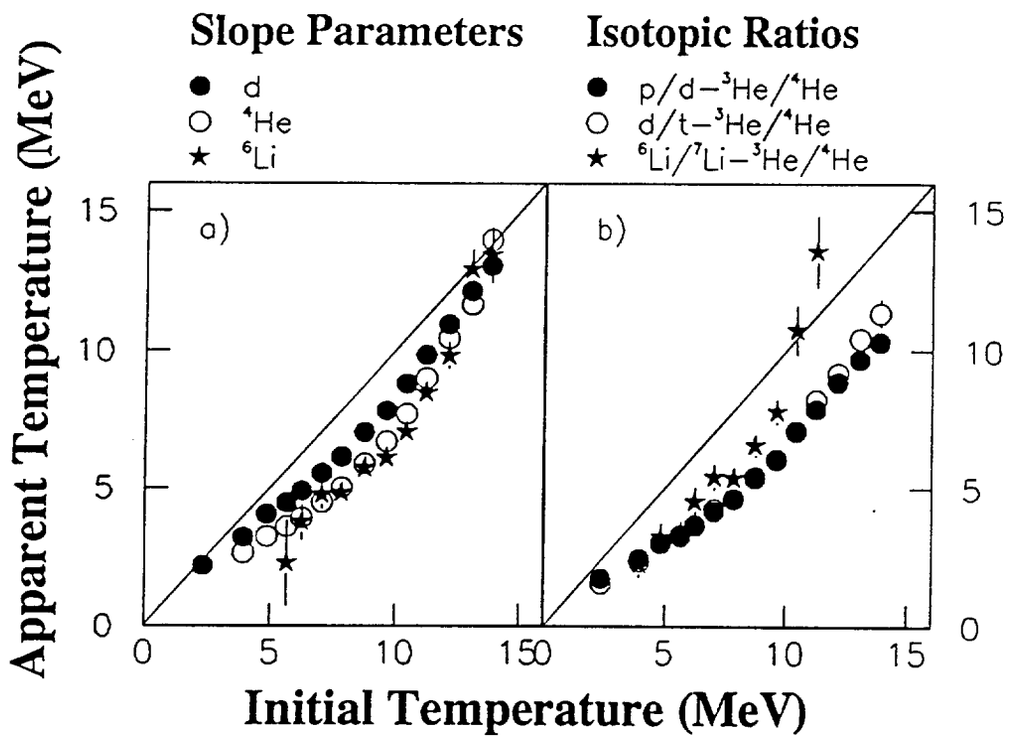
Slope Parameters
d
4He
6Li
Isotopic Ratios
p/d−3He/4He
d/t−3He/4He
6Li/7Li−3He/4He
a)
b)
Apparent Temperature (MeV)
Initial Temperature (MeV)
0
5
10
15

Fig. 4

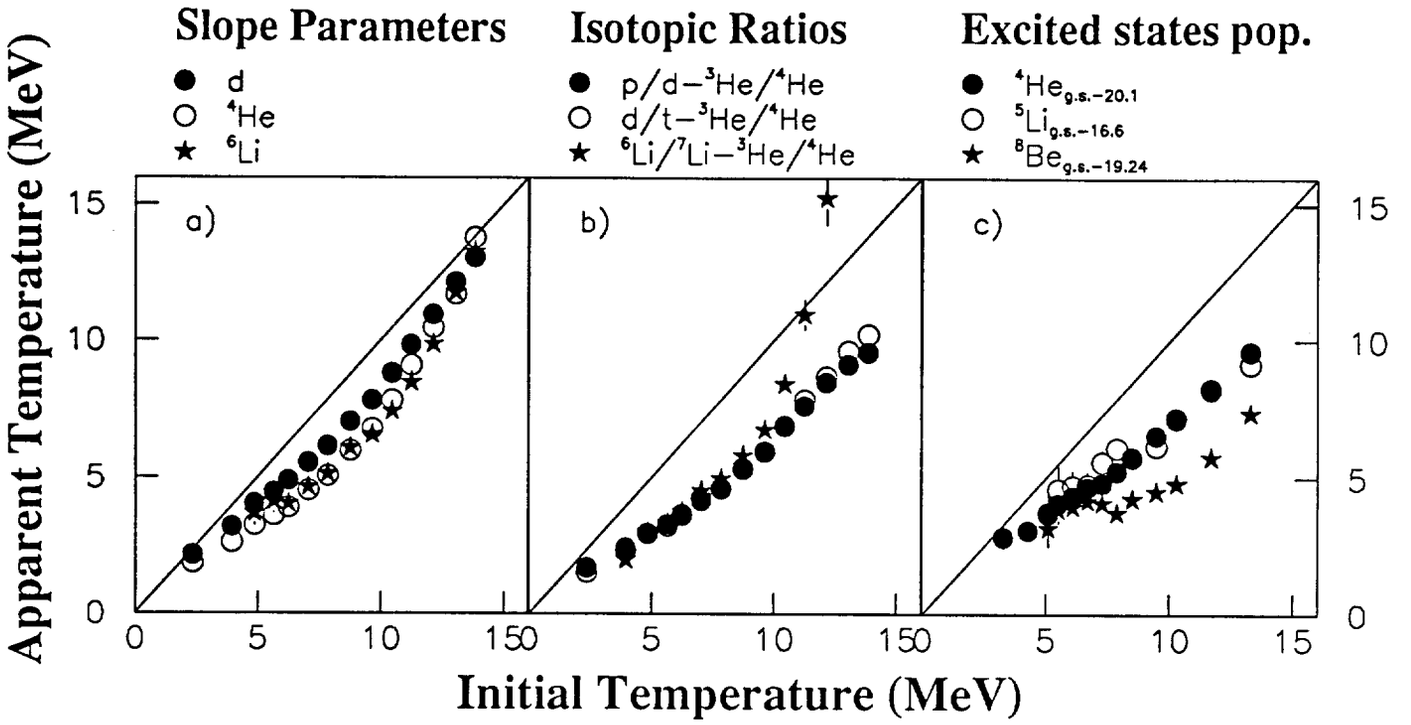
Slope Parameters
d
4He
6Li
Isotopic Ratios
p/d−3He/4He
d/t−3He/4He
6Li/7Li−3He/4He
Excited states pop.
4He g.s.−20.1
5Li g.s.−16.6
8Be g.s.−19.24
a)
b)
c)
Apparent Temperature (MeV)
Initial Temperature (MeV)
0
5
10
15
150

Fig. 5

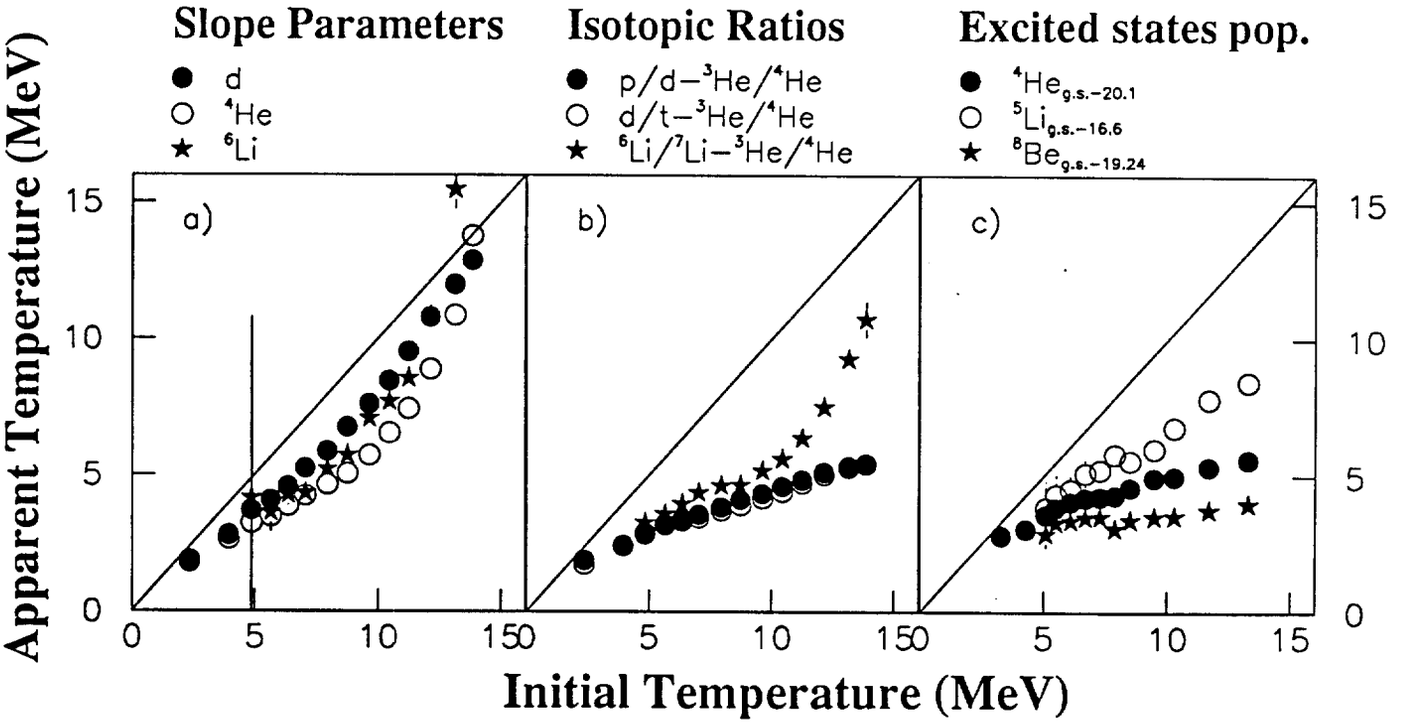
Slope Parameters
d
4He
6Li
Isotopic Ratios
p/d−3He/4He
d/t−3He/4He
6Li/7Li−3He/4He
Excited states pop.
4He g.s.−20.1
5Li g.s.−16.6
8Be g.s.−19.24
a)
b)
c)
Apparent Temperature (MeV)
Initial Temperature (MeV)
0
5
10
15
150

Fig. 6

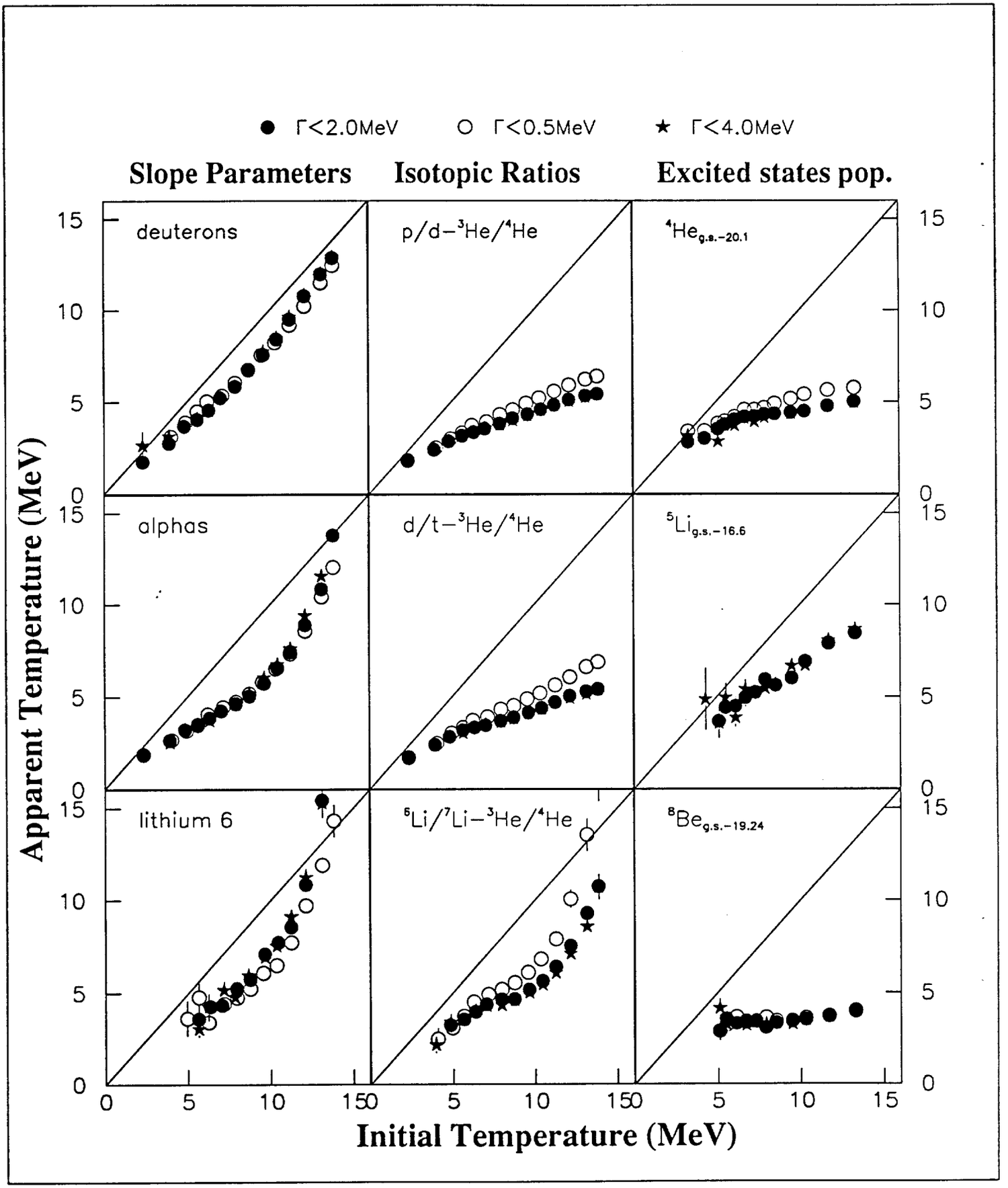
● Γ<2.0MeV
○ Γ<0.5MeV
★ Γ<4.0MeV
Slope Parameters
Isotopic Ratios
Excited states pop.
deuterons
p/d−3He/4He
4He g.s.-20.1
alphas
d/t−3He/4He
5Li g.s.-16.6
lithium 6
6Li/7Li−3He/4He
8Be g.s.-19.24
Apparent Temperature (MeV)
Initial Temperature (MeV)
0
5
10
15

Fig. 7

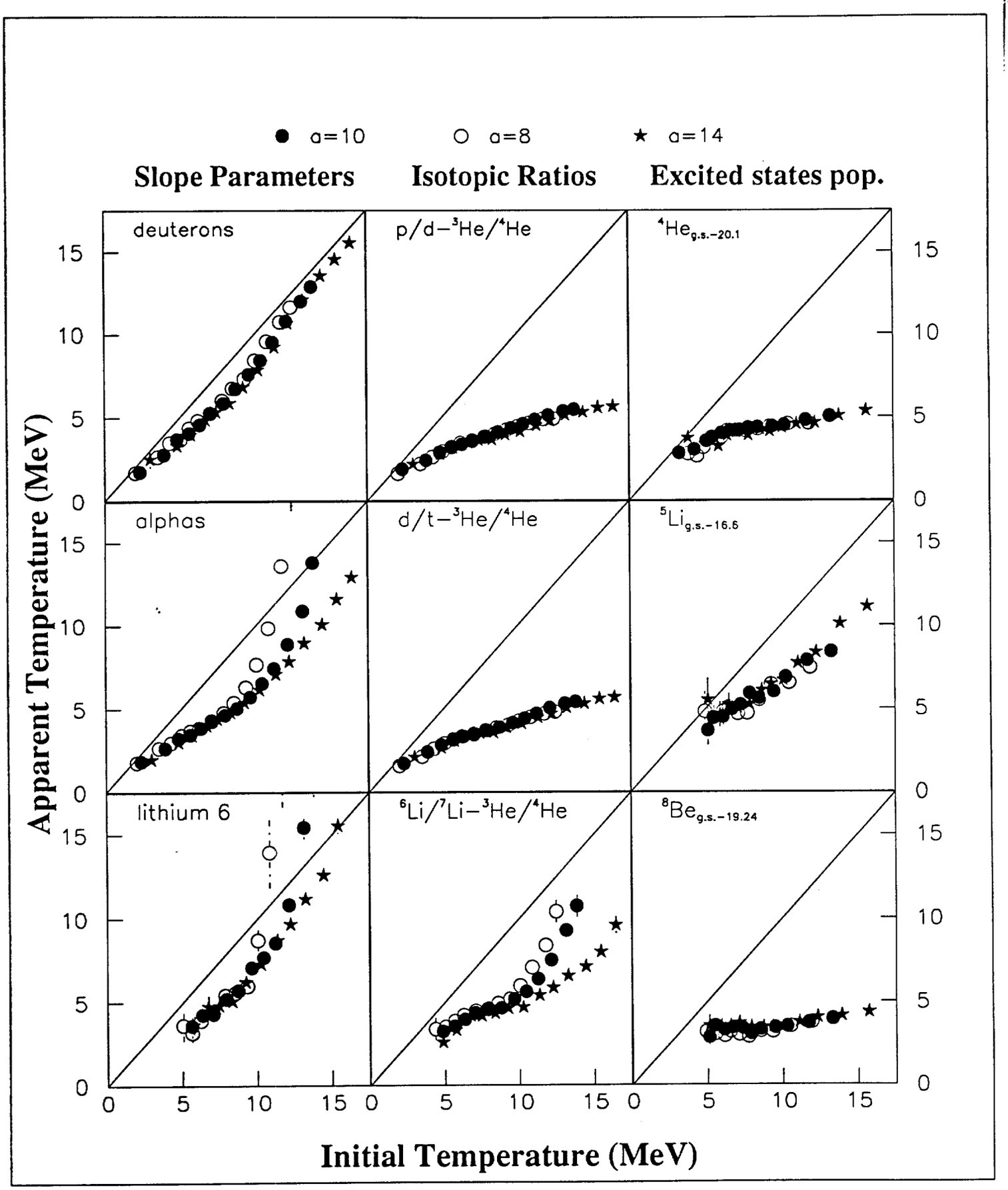
● a=10
○ a=8
★ a=14
Slope Parameters
Isotopic Ratios
Excited states pop.
deuterons
p/d−³He/⁴He
⁴He g.s.−20.1
alphas
d/t−³He/⁴He
⁵Li g.s.−16.6
lithium 6
⁶Li/⁷Li−³He/⁴He
⁸Be g.s.−19.24
Apparent Temperature (MeV)
Initial Temperature (MeV)
0
5
10
15

Fig. 8

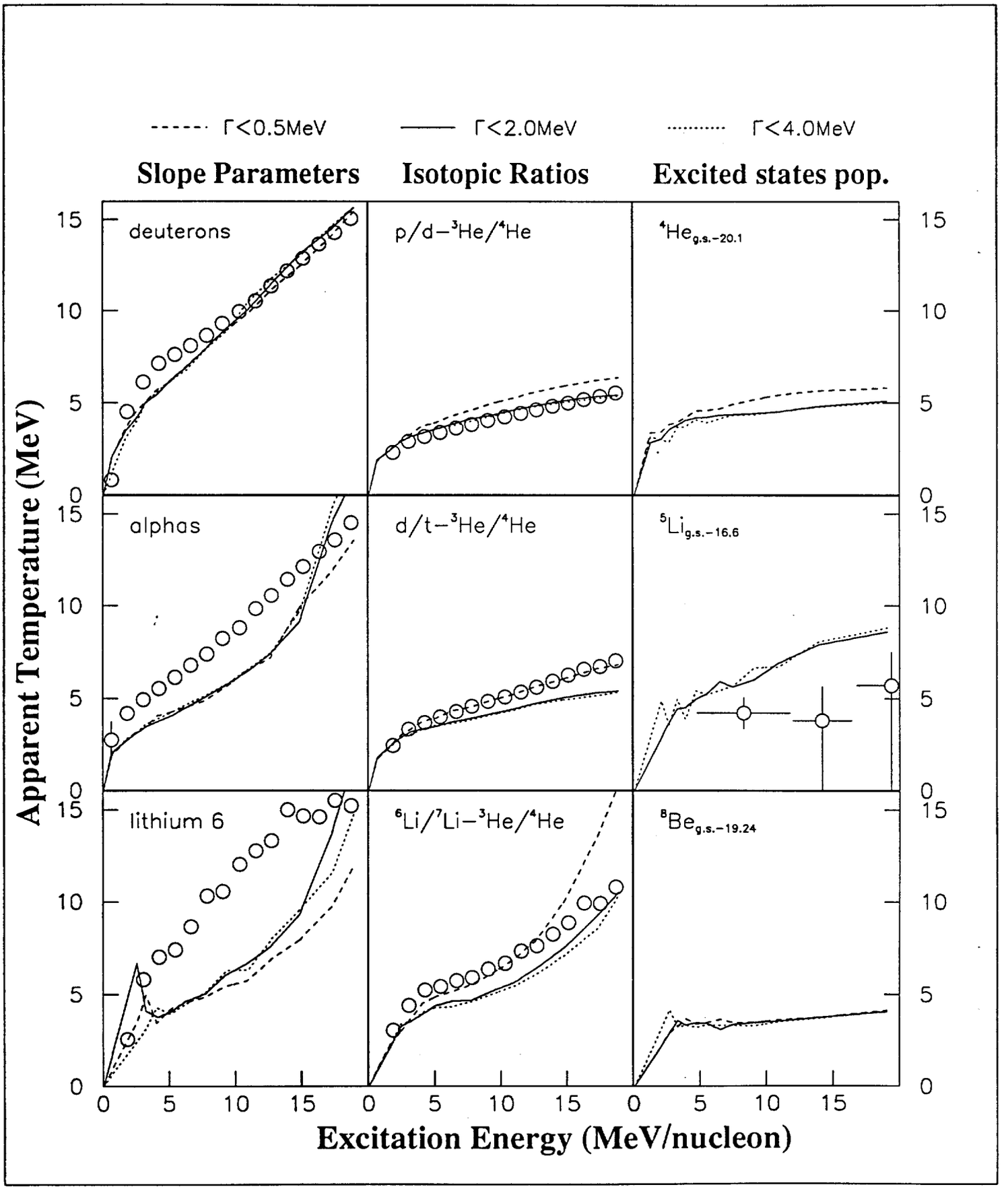
Γ<0.5MeV
Γ<2.0MeV
Γ<4.0MeV
Slope Parameters
Isotopic Ratios
Excited states pop.
deuterons
p/d−³He/⁴He
⁴He g.s.−20.1
alphas
d/t−³He/⁴He
⁵Li g.s.−16.6
lithium 6
⁶Li/⁷Li−³He/⁴He
⁸Be g.s.−19.24
Apparent Temperature (MeV)
Excitation Energy (MeV/nucleon)
0
5
10
15

Fig. 9

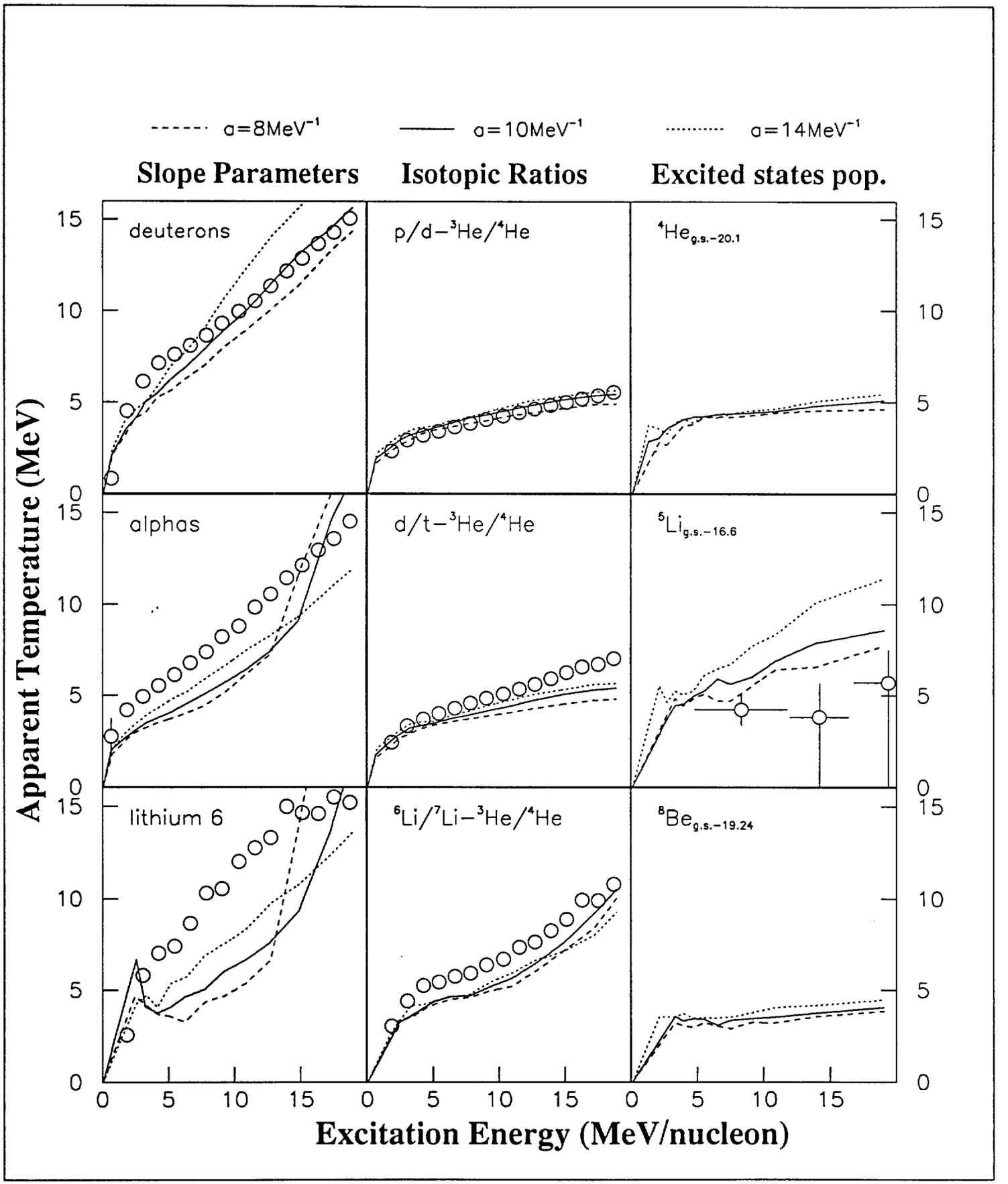
a=8MeV⁻¹
a=10MeV⁻¹
a=14MeV⁻¹
Slope Parameters
Isotopic Ratios
Excited states pop.
deuterons
p/d−³He/⁴He
⁴He g.s.−20.1
alphas
d/t−³He/⁴He
⁵Li g.s.−16.6
lithium 6
⁶Li/⁷Li−³He/⁴He
⁸Be g.s.−19.24
Apparent Temperature (MeV)
Excitation Energy (MeV/nucleon)
0
5
10
15

Fig. 10

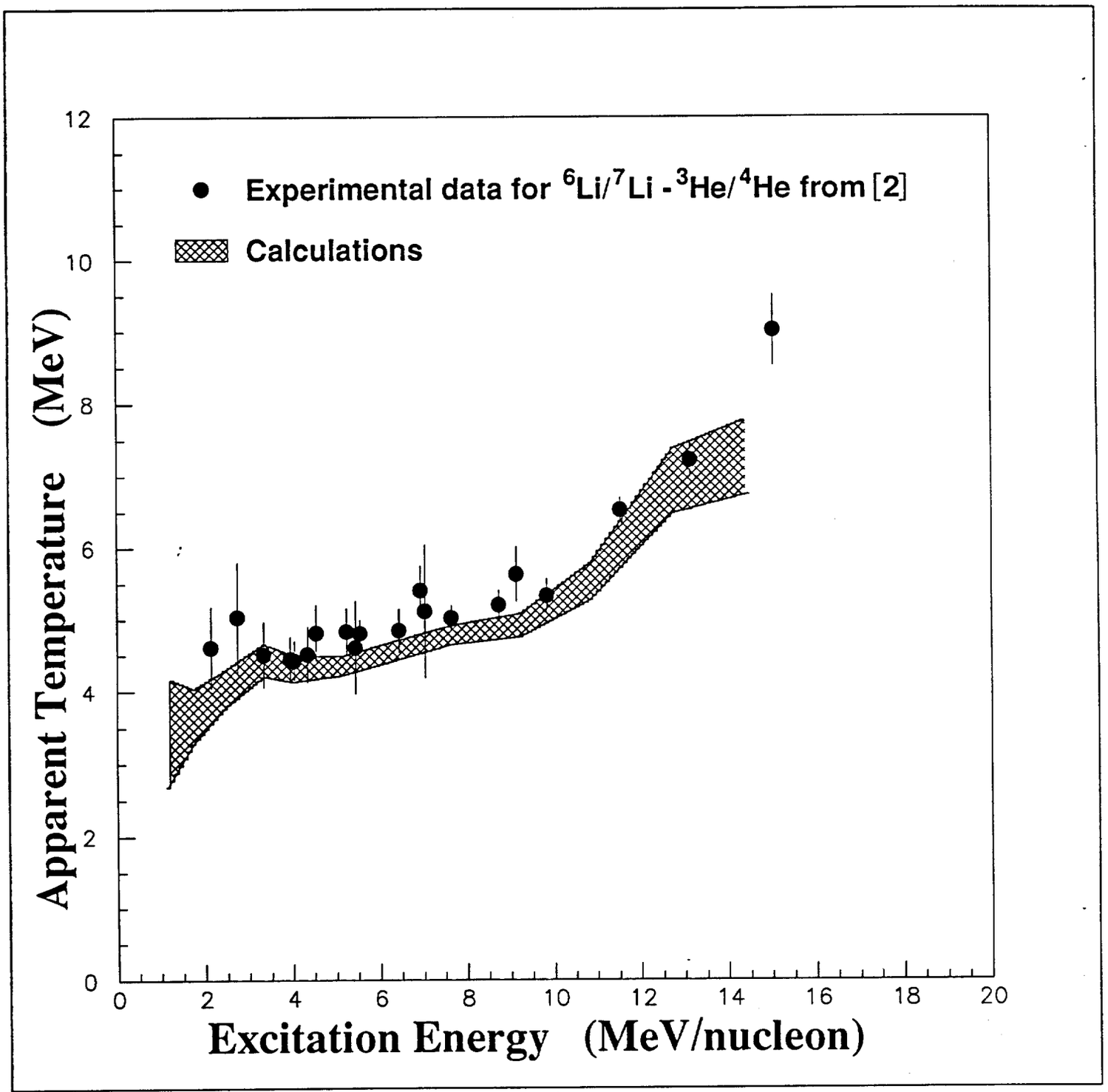
Experimental data for $^{6}Li/^{7}Li$ - $^{3}He/^{4}He$ from [2]
Calculations
Apparent Temperature (MeV)
Excitation Energy (MeV/nucleon)
0
2
4
6
8
10
12
14
16
18
20

Fig. 11

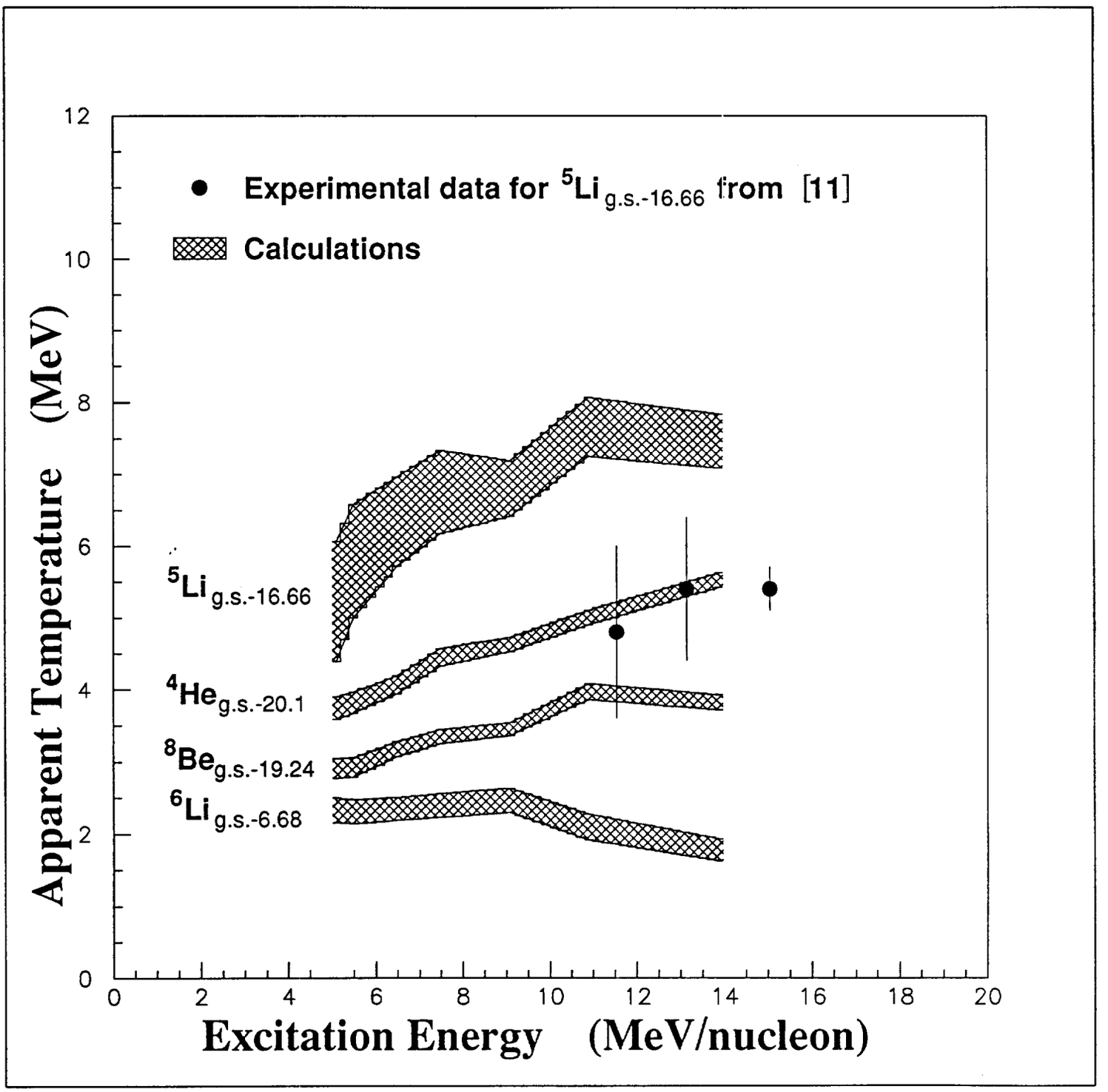
Experimental data for $^{5}Li_{g.s.-16.66}$ from [11]
Calculations
$^{5}Li_{g.s.-16.66}$
$^{4}He_{g.s.-20.1}$
$^{8}Be_{g.s.-19.24}$
$^{6}Li_{g.s.-6.68}$
Apparent Temperature (MeV)
Excitation Energy (MeV/nucleon)
0
2
4
6
8
10
12
14
16
18
20

Fig. 12